Controlled Iron-Doping of Macrotextured Nanocrystalline Titania

Yuhong Zhang,[†,||] Stefan G. Ebbinghaus,[†] Anke Weidenkaff,[†] Thomas Kurz,[‡] Hans-Albrecht Krug von Nidda,[‡] Peter J. Klar,*[,§] Martin Güngerich,[§] and Armin Reller[†]

Solid State Chemistry and Experimental Physics V, Electronic Correlations and Magnetism, Institute of Physics, University of Augsburg, 86135 Augsburg, Germany, Department of Physics and Material Sciences Center, Philipps University, 35032 Marburg, Germany, and Department of Chemistry, Zhejiang University, 310027 Hangzhou, China

Received April 8, 2003. Revised Manuscript Received August 25, 2003

Titanium dioxide, despite its rather simple summation formula, is a material with widespread applications. Fe-doped TiO_2, because of its photocatalytic properties, is employed in devices for water detoxification, water splitting, and air purification, as well as for solar cells. For each application, its functionality can be optimized by adjusting the crystal modification by the degree of Fe doping and by structuring on atomic to macroscopic length scales. We have developed a flexible and inexpensive butanediol sol−gel synthesis for Fe-doped titania which allows us to control the material properties on atomic, mesoscopic, and macroscopic scales with respect to structure−morphology property relationships, i.e., to generate a tailor-made functional material. A kinetic phase diagram of TiO_2:Fe based on this synthesis pathway, in particular with respect to Fe incorporation, has evolved as a result of the application of a large set of complementary means of investigation.

Introduction

Titanium dioxide is, to date, not only the most important synthetic pigment,[1−3] but also, due to its outstanding electronic properties, one of the most photoactive, and, because of its high chemical stability and nontoxicity, one of the most practical materials employed in heterogeneous photocatalysis.[4−6] Extensive research is in progress for exploring its widespread applications such as water detoxification, water splitting, air purification, and solar cells.[7,8] The catalytic properties of titania depend on its crystal modification and crystallinity, and can be further tuned by doping and by structuring. The rutile phase, for example, is very efficient as a catalyst for decomposing H_2S, whereas the anatase phase is more active in many other catalytic processes.[6] Doping with transition metals allows a tuning of the absorption properties[9] of TiO_2. The key dopant is Fe.[9,10] A huge surface enhancement and thus an increase of the reactivity can be obtained by nanostructuring.[11] Here, we demonstrate how the material properties of iron-doped titania can be tuned from the macroscopic level down to the microscopic level by varying the synthesis conditions of a rather inexpensive butanediol sol−gel fabrication process.

Three different crystalline structures are known for pure TiO_2. At ambient conditions, the tetragonal rutile structure is thermodynamically stable. Tetragonal anatase and orthorhombic brookite transform irreversibly into rutile when heated. The phase-transition temperature depends on the size of the crystallites at least for the anatase−rutile transition.[12] To our knowledge, all previous magnetic experiments concerning iron-doping of TiO_2 have been performed with samples containing less than 0.2% of iron atoms.[17,19,20] If iron atoms are incorporated into TiO_2 in this dilute regime they are in

* Corresponding author. Phone: ++49 (0)6421 2821354. Fax: ++49 (0)6421 2827036. E-mail: klarp@mailer.uni-marburg.de.
† Solid State Chemistry, Institute of Physics, University of Augsburg.
‡ Experimental Physics V, Electronic Correlations and Magnetism, Institute of Physics, University of Augsburg.
§ Department of Physics and Material Sciences Center, Philipps University.
|| Department of Chemistry, Zhejiang University.

(1) Adams, R. *Eur. Coatings J.* **1996**, *6*, 395.
(2) Buxbaum, G., Ed. *Industrial Inorganic Pigments*; VCH: Weinheim, Germany, 1993.
(3) Rentschler, T.; Reller, A. *Eur. Coatings J.* **1999**, *4*, 80.
(4) Linsebigler, A. L.; Guangquan, L.; Yates, J. T., Jr. *Chem. Rev.* **1995**, *95*, 735.
(5) Fujishima, A.; Rao, T. N.; Tryk, D. A. *J. Photochem. Photobiol., C* **2000**, *1*, 1.
(6) Mills, A.; Le Hunte, S. *J. Photochem. Photobiol., A* **1997**, *108*, 1.
(7) Grätzel, M. *CATTECH* **1999**, *3*, 4.
(8) Shklover, V.; Nazeeruddin, M.-K.; Zakeeruddin, S. M.; Barbe, C.; Kay, A.; Haibach, T.; Steurer, W.; Hermann, R.; Nissen, H.-U.; Grätzel, M. *Chem. Mater.* **1997**, *9*, 430.
(9) Litter, M. I.; Navio, J. A. *J. Photochem.Photobiol., A* **1996**, *98*, 171.
(10) Rusina, O.; Linnik, O.; Eremenko, A.; Kisch, H. *Chem. Eur. J.* **2003**, *9*, 561.
(11) Fröba, M.; Muth, O.; Reller, A. *Solid State Ionics* **1997**, *101−103*, 249.
(12) Ma, W.; Lu, Z.; Zhang, M. *Appl. Phys. A* **1998**, *66*, 621.
(13) Beattie, I. R.; Gilson, T. R. *Proc. R. Soc. A* **1968**, *307*, 407.
(14) Porto, S. P. S.; Fluery, P. A.; Damen, T. C. *Phys. Rev.* **1967**, *154*, 522.
(15) Bersani, D.; Lottici, P. P.; Montenero, A. *J. Mater. Sci.* **2000**, *35*, 4301.
(16) Shannon, R. D.; Pask, J. A. *J. Am. Ceram. Soc.* **1965**, *48*, 391.
(17) Horn, M.; Schwerdtfeger, C. F. *Solid State Commun.* **1970**, *8*, 1741.
(18) Castner, T.; Newell, G. S.; Holton, W. C.; Slichter, C. P. *J. Chem. Phys.* **1960**, *32*, 668.

10.1021/cm034246p CCC: $25.00
Published on Web 09/30/2003

the Fe^{3+} state without exception. Titania modifications with higher Fe content have been widely reported. However, to our knowledge, no experiments were performed to probe the local Fe coordination, i.e., to prove unambiguously that Fe substitutes Ti while conserving the TiO_2 modification. Here, we present a comprehensive study of Fe in TiO_2 for significantly higher concentrations. We clarify by magnetic as well as spectroscopic techniques the site-specific incorporation of Fe in rutile and anatase. Furthermore, we demonstrate that single-phase material with Fe contents up to 0.2% and 30% in rutile and anatase, respectively, are stable even at high temperatures. These single-phase compounds can be obtained reproducibly only by soft chemistry synthesis pathways.

Experimental Methods

For the synthesis of the nanostructured iron-doped titania a modified sol−gel method was applied. To a solution of $Fe(NO_3)_3 \cdot 9H_2O$ (>98%, Merck) in butanediol (>98%, Merck) titanium isopropoxide (98%, Aldrich) was added at room temperature under constant stirring. The molar ratio of butanediol and titanium isopropoxide was 1:2. Textile sheets were soaked with the precursor solution and dried at ambient temperature for 5 d. The template containing the dry gel was calcinated in air at the temperatures mentioned in the text.

The morphology of the samples was examined using a LEO Gemini 982 scanning electron microscope (SEM) equipped with a Röntec energy-dispersive X-ray analysis (EDX) detector system.

Transmission electron microscopic (TEM) studies were performed on a Phillips CM 30 instrument equipped with energy dispersive X-ray analysis (EDX) and a selected-area electron diffraction (SAED) detector.

The surface area and pore size distribution were measured by the BET method (Micrometrics ASAP 2000).

XRD measurements were done on a Seifert TT3003 diffractometer operating with Cu Kα radiation. Diffraction patterns were recorded in the angular range $20° \leq 2\theta \leq 80°$ with a stepwidth of 0.02° and a counting time of 1 s per data point.

Unpolarized Raman measurements were performed in backscattering geometry using a Jobin Yvon micro-Raman system based on an Olympus BX41 optical microscope. Excitation light (514.5 nm) of an Ar^+ laser (Coherent Innova 200) was coupled via optical fibers into the microscope system and focused onto the sample. The laser power on the sample was less than 20 mW to avoid laser-induced annealing. The scattered light was collected via the microscope objective. Elastically scattered light was rejected by a Kaiser Optics holographic Notch filter before coupling the Raman scattered light into the spectrometer system (Acton Research Corporation SpectraPro-500). The spectra were detected by a liquid-nitrogen cooled ISA CCD2000 CCD camera.

The EXAFS measurements were done at the beamline E4 of HASYLAB at DESY in transmission mode at room temperature. The spectra were energy-calibrated against the first inflection point of the K edge spectra of Fe or Ti metal. After removing the background, which was approximated by a Victoreen function in the pre-edge region, and normalization of the edge height, the photon energy (E) to wave vector (k) conversion was carried out using the first inflection point of the absorption edge as energy threshold. The atomic absorption was subtracted by fitting the k^2 weighted spectra in the range $2.15\ Å^{-1} < k < 12.5\ Å^{-1}$ for Fe (and $2.4\ Å^{-1} < k < 15\ Å^{-1}$ for Ti) with a fifth-degree polynomial function. For the Fourier transformation the data were weighted with a Bessel Window ($\beta = 4$).

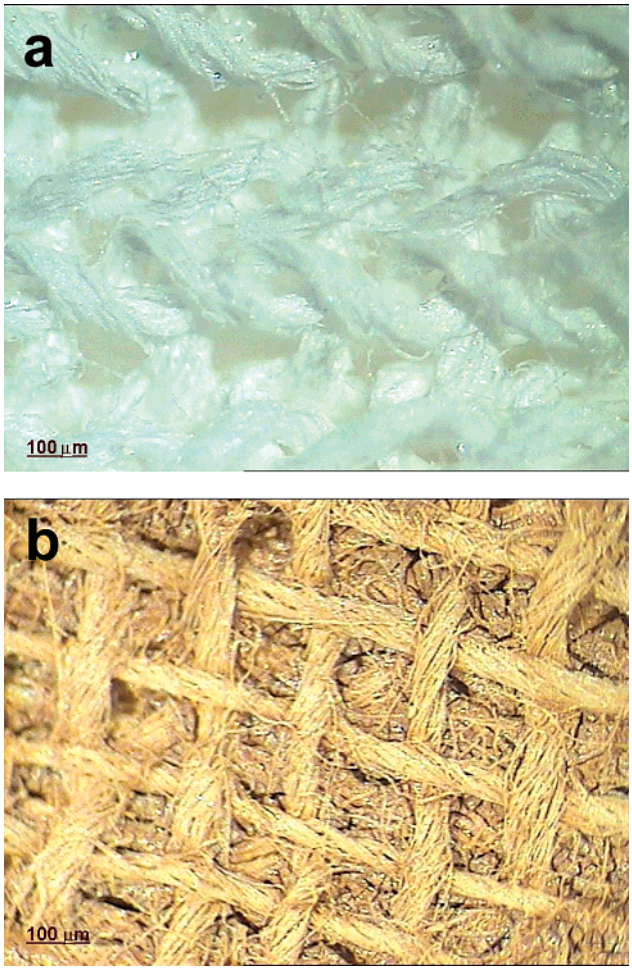

Figure 1. Photographs of a macroscopic sheet of (a) pure and (b) iron-doped titania.

EPR measurements were performed in a Bruker Elexsys 500 CW spectrometer at X-band frequencies (9.48 GHz) and magnetic fields up to 1 T between 4 and 300 K in a continuous-flow He cryostat (Oxford Instruments). EPR measures the microwave absorption $P_{abs}(B)$ of a paramagnetic sample dependent on the external magnetic field B. To improve the signal-to-noise ratio the field derivative dP_{abs}/dB was detected by lock-in technique with field modulation.

The magnetization was measured in a commercial superconducting quantum interference device (SQUID) magnetometer (Quantum Design) working in magnetic fields up to 5 T and at temperatures between 1.8 and 400 K.

Results and Discussion

Color photographs of macrotextured sheets of pure titania and iron-doped titania are shown in Figure 1a and b, respectively. The change of color of the sheets demonstrates how the absorption properties of the material can be tuned by iron doping. The macroscopic texture is controlled by the type of cellulose or cotton fiber network used as template in the sol−gel process. A control of the texture on this macroscopic level will be crucial for technical applications, e.g., when employing such material in water-purification devices.

In the following we will focus on the intrinsic mesoscopic and microscopic properties of iron-doped TiO_2 synthesized by the butanediol sol−gel process. For this purpose, we have prepared crystalline samples using

(19) de Biasi, R. S.; Grillo, M. L. N. *J. Phys. Chem. Solids* **1996**, *57*, 137.
(20) Kim, S. S.; Jun, S. S.; Park, M. J. *J. Korean Phys. Soc.* **1990**, *23*, 73.

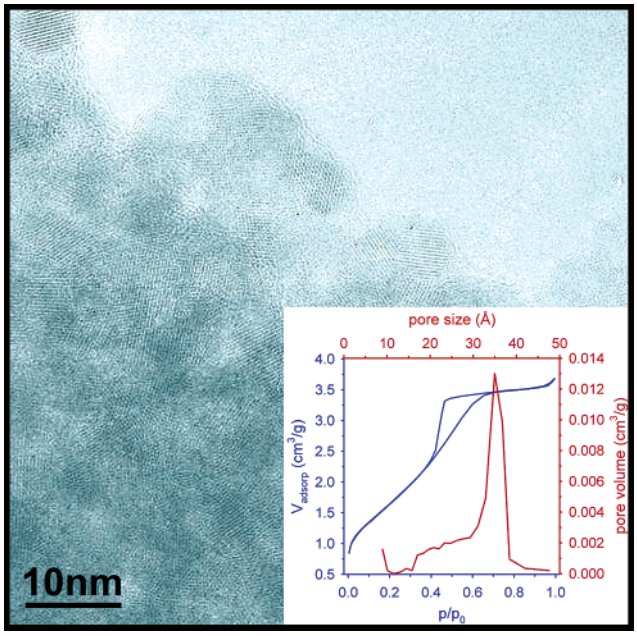

Figure 2. TEM image of the mesoporous structure of an iron-doped anatase sheet. Inset: BET isotherms and the corresponding pore size distribution.

the same synthesis pathway as for the macrostructured samples, but without sheet templates.

Figure 2 is an HRTEM image of the nanoscopic structure of a pure anatase crystallite calcinated at T_c = 600 °C showing the homogeneous size distribution of grains and pores with an average of 4−5 nm, which was confirmed by sorption measurements (BET method). The inset shows the pore size distribution deduced from BET isotherms and the Kelvin equation. For this sample the pore size is about 4 nm and the size distribution is very narrow. A size control of the pores is desirable as it allows a controlled enhancement of the active surface and might help to avoid filling of the pores with contaminants, which would lead to degradation of the catalytic properties. According to the HRTEM lattice images and SAED pattern the crystalline part of the samples consists of anatase as dominant phase and rutile in traces. Furthermore, small amorphous regions are visible.

Raman and XRD measurements were performed to identify the crystalline phases synthesized by the sol−gel process at calcination temperatures ranging from 300 to 800 °C and nominal Fe concentrations up to 30%. As an example, Figure 3a shows the analysis of an XRD pattern of a TiO_2:Fe 10% sample calcinated at T_c = 630 °C. A quantitative phase analysis yielded a composition of 75% anatase, 10% rutile, and 15% pseudobrookite (Fe_2TiO_5), another phase of the TiO_2:Fe system. The modeled traces are the top three curves in the figure labeled A, R, and P. Below, the experimental curve and fit are compared. The difference between experimental and modeled trace is shown as the lowest curve.

If one assumes that all Fe ions are embedded in the pseudobrookite phase at this temperature, the expected weight percentage of this compound is 15%. The observed composition matches this value very well, indicating that only small amounts of iron can be present in rutile or anatase at temperatures above 600 °C, in

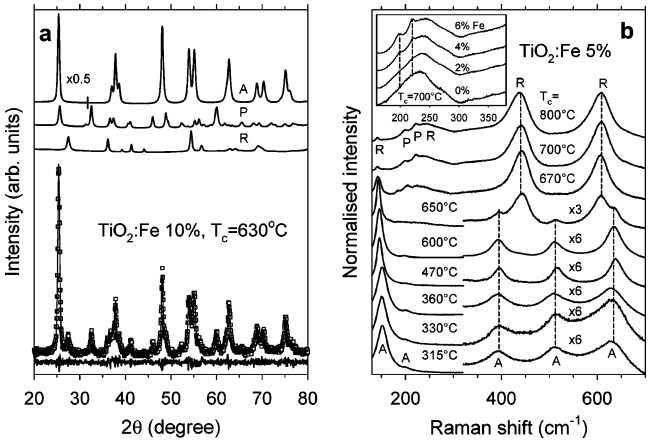

Figure 3. Phase transition from doped anatase (A) to rutile (R) and pseudobrookite (P) monitored by XRD and Raman spectroscopy. (a) XRD pattern of TiO2:Fe 10% after calcinating at 630 °C and a corresponding fit. The contributions of anatase, rutile, and pseudobrookite are shown in the upper part of the graph, and the difference between experimental and modeled trace is shown at the bottom of the graph. (b) Room-temperature Raman spectra of TiO_2:Fe 5% calcinated at various temperatures. Features due to the anatase, rutile, and pseudobrookite phases are indicated. High-frequency peaks have been connected by vertical dashed lines. High-frequency regions in the spectra samples synthesized at low temperatures have been magnified with respect to the corresponding low-frequency regions for clarity. Inset: room-temperature Raman spectra of TiO_2:Fe with different iron concentrations calcinated at 700 °C. The evolution of the pseudobrookite features has been indicated by vertical dashed lines.

agreement with the EPR and EXAFS results discussed below.

Figure 3b shows a series of Raman spectra of TiO_2:Fe samples calcinated at different temperatures and with a nominal iron content of 5%. Anatase single crystals have Raman-active phonons at 144 cm^{-1} (E_g), 197 cm^{-1} (E_g), 399 cm^{-1} (B_{1g}), 513 cm^{-1} (A_{1g}), 519 cm^{-1} (B_{1g}), and 639 cm^{-1} (E_g).[13] All these phonon modes are clearly visible in the spectra of low-temperature samples (from 315 up to 600 °C), and despite the considerable iron doping they are practically unshifted compared to the spectra of the pure TiO_2 samples. The features observed in the spectra of the high-temperature samples (700 and 800 °C) correspond to Raman-active phonons of rutile single crystals which have been reported to occur at wavenumbers of 143 cm^{-1} (B_{1g}), 447 cm^{-1} (E_g), 612 cm^{-1} (A_{1g}), and 826 cm^{-1} (B_{2g}).[14] These are also nearly unshifted. The broad shoulder around 240 cm^{-1} has been reported for rutile in the literature.[14] In the spectra of the high-temperature samples, the evolution of two additional Raman peaks at 195 and 220 cm^{-1} is observed with increasing iron content. The inset of Figure 3b shows a series of spectra from samples calcinated at the same temperature of 700 °C but containing different amounts of Fe. The two signals are due to pseudobrookite, indicating that a segregation occurs at higher temperatures.[15] The phase transition from anatase into the mixed phase of rutile and pseudobrookite takes place between 600 and 650 °C. This is a significantly lower temperature than the one observed for the anatase−rutile transition in TiO_2 single crystals (≥900 °C).[16] The decrease of the phase-transition temperature is known to be characteristic of TiO_2 nano-

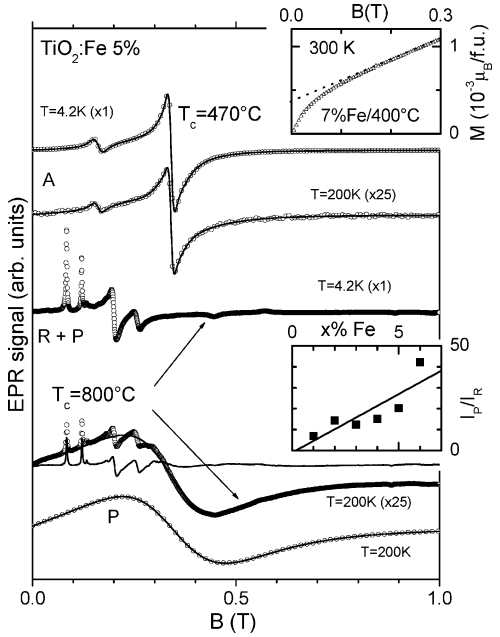

Figure 4. EPR spectra at 4.2 and 200 K for TiO_2:Fe 5% calcinated at 470 °C (first and second) and 800 °C (third and fourth), respectively, and EPR spectrum of Fe_2TiO_5. Solid lines are fit curves as described in the text. For the fourth spectrum also the result after subtraction of the fit curve is shown as a solid line. The relative amplification factors between temperatures of the same sample are given in brackets. Upper inset: SQUID magnetization for TiO_2:Fe 7% calcinated at 400 °C. The dotted line indicates the extrapolation of the spontaneous moment. Lower inset: ratio of the intensities of pseudobrookite and rutile phase normalized to the respective Curie−Weiss law. The solid line indicates the fit $(x - x_c)/x_c$ to determine the critical concentration x_c of Fe^{3+} in rutile.

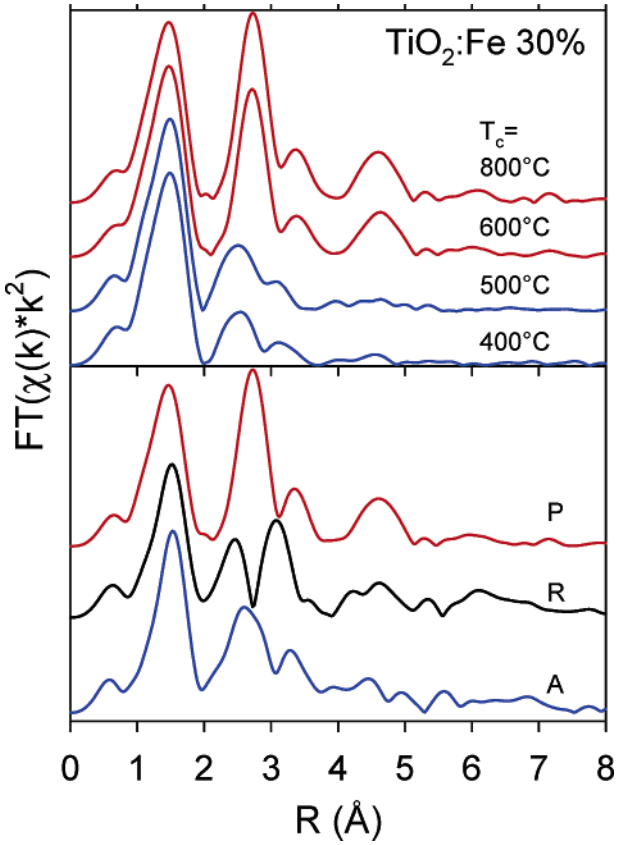

Figure 5. Upper panel: modified radial distribution functions (mRDF) of iron in 30% Fe-doped TiO_2 calcinated at different temperatures. Lower panel: mRDFs of the reference samples pseudobrookite (P), rutile (R), and anatase (A). The latter two compounds were measured at the Ti−K threshold.

crystals and has been attributed to surface effects.[12] The Raman results basically confirm the XRD results.

EPR and EXAFS measurements are used to identify the distribution of the Fe-dopants between the three phases of the TiO_2:Fe system, namely anatase, rutile, and pseudobrookite. The results are presented in Figures 4 and 5. EPR directly probes the Fe^{3+} spin ($S = 5/2$) and hence gives information about the local symmetry of the host material. As one can see from the example TiO_2:Fe 5% presented in Figure 4, the resonance spectra exhibit characteristic features, which allow one to distinguish unambiguously between the three phases of the TiO_2:Fe system. The upper two spectra are typical of the samples calcinated at 470 °C. These spectra could be best fitted by four Lorentzian lines: i.e., two lines with a g value near $g = 2.0$, another resonance at $g = 4.2$, and an additional very broad underlying line (line width > 0.3 T) with a resonance field between 0.2 and 0.3 T. The intensity of the whole spectrum exhibits a Curie−Weiss-like decrease, except for the very broad line with a nearly temperature-independent intensity.

The two overlapping lines observed at $g = 2.0$ with line widths of 0.01 and 0.04 T can be ascribed to Fe^{3+} ions in the anatase structure. They result from the powder-average of the anisotropic EPR spectrum, which has been reported for anatase single crystals[17] with a dominant uniaxial zero-field splitting $D = 308.7 \cdot 10^{-4}$ cm^{-1}. The weak line at $g = 4.2$ probably indicates the presence of a small residual amount of the amorphous TiO_2 phase, which appears at low calcination temperatures <400 °C, as such a signal is typical of Fe^{3+} in glass.[18] The broad underlying line can be ascribed to traces of metallic iron clusters, which were identified by additional magnetization measurements, shown in the upper inset of Figure 4. The magnetization curve reveals a spontaneous moment of $0.4 \cdot 10^{-3}$ μ_B per formula unit (μ_B = Bohr magneton), which corresponds to less than 0.1% Fe clusters. These observations prove that the vast majority of the Fe ions are incorporated into the anatase structure. The third and fourth spectra, shown in Figure 4, were obtained from samples calcinated at 800 °C. The spectrum measured at 4.2 K reveals a complicated structure with several sharp lines, which has been already reported for powder spectra of Fe^{3+} in rutile[19] and was intensively studied in single crystals[20] as well. With increasing temperature a broad line develops in addition to the low-temperature spectrum, as one can see from the data taken at 200 K. This broad line is typical of pseudobrookite which is shown as the fifth spectrum acquired at 200 K. The resonance line of pseudobrookite, which is well described by a single Lorentz curve, strongly broadens with decreasing temperature and becomes undetectable below 100 K on approaching the spin-glass transition.[21] Therefore, it cannot be observed in the rutile spectrum at 4.2 K.

(21) Atzmony, U.; Gurewitz, E.; Melamud, M.; Pinto, H.; Shaked, H.; Gorodetsky, G.; Hermon, E.; Hornreich, R. M.; Shtrikman, S.; Wanklyn, B. *Phys. Rev. Lett.* **1979**, *43*, 782.

After subtraction of the pseudobrookite line from the 200 K rutile spectrum, only the features of the 4 K spectrum remain, as it is also shown together with the fourth spectrum in Figure 4. Comparing the ratio of the EPR intensities between the pseudobrookite (I_P) and the rutile (I_R) signal for several nominal Fe^{3+} concentrations, we were able to estimate the critical amount, x_c, of Fe^{3+}, which can be incorporated into the rutile phase, as $x_c \approx 0.2\%$. This is indicated by the solid line in the lower inset of Figure 4, where the concentration dependence of the intensity ratio was fitted by $I_P/I_R = (x - x_c)/x_c$. The intensities were calculated from the areas under the spectra by 2-fold integration of the EPR signal and normalized by the Curie−Weiss law $(T - \Theta_{CW})^{-1}$, with $\Theta_{CW} = 0$ K for diluted iron in rutile and $\Theta_{CW} = -350$ K for Fe_2TiO_5, determined from the temperature dependence of the EPR intensity. From the analysis of the EPR data, the rutile structure allows for only 0.2% Fe^{3+} to occupy regular lattice sites, whereas the pure anatase structure is unambiguously identified up to 3% Fe^{3+}. For more than 3% Fe^{3+} the spectra still bear the characteristics of the anatase phase. But the exchange interaction between the Fe^{3+} ions gains more and more influence with increasing concentration, and, hence, the EPR intensity exhibits deviations from the pure Curie law. An extrapolation of the high-temperature part of the inverse intensity yields Curie−Weiss temperatures comparable to that of pseudobrookite, however this may be just due to the higher Fe concentration within the anatase phase. Finally, above 10% Fe^{3+} the EPR signal shows an additional line broadening which makes it impossible to distinguish unambiguously between the anatase phase and pseudobrookite. At these high Fe concentrations EPR is not the appropriate method for determining the purity of the phases, because the spectra are governed by the strong correlations between the Fe spins. To extend our investigations to samples with higher nominal Fe concentrations, we used EXAFS. The two methods complement each other: both EPR and EXAFS yield information about oxidation states and the local environment of the iron centers. EPR is much more sensitive than EXAFS and can therefore be used for samples with low Fe concentrations. Because of the strong spin−spin interactions mentioned above, EPR is not the method of choice for higher Fe contents. EXAFS, on the other hand, is less sensitive but has no upper concentration limit. Therefore, we used this method for investigations of the samples with Fe concentrations up to 30%.

In Figure 5, the upper panel shows the modified radial distribution functions (mRDF), i.e., the Fourier transforms of the k^2-weighted EXAFS functions, obtained from Fe−K edge measurements of 30% Fe-doped samples calcinated at different temperatures. For comparison, the lower panel depicts mRDFs of an Fe_2TiO_5 reference sample (prepared by conventional solid-state reaction) and of undoped anatase and rutile, respectively. The Fe_2TiO_5 data were taken at the Fe−K threshold, whereas the two TiO_2 modifications were measured at the Ti−K absorption edge.

One might be concerned whether pure anatase and rutile are appropriate references for Fe-doped titania because both the absorbing atom and the chemical environment are different: for the pure titanates EXAFS measurements were performed at the Ti threshold and Ti is the only backscattering transition metal. The substituted samples, on the other hand, were measured at the Fe-edge and the backscatterers are both Ti and Fe. Fortunately, it is a well-established fact that the central atom phase shift and the backscattering atom phase shift, as well as the backscattering amplitude, change slowly and smoothly with the atomic number Z.[22] For this reason the EXAFS signals for elements with similar Z (e.g., the series of 3d-transition metals) are comparable, and backscattering contributions of iron and titanium show little differences. We verified this assumption by performing additional Ti−K edge EXAFS measurements for the Fe_2TiO_5 reference and the 30% doped sample calcinated at 400 °C (i.e., below the phase transition described below). As expected, the mRDFs at the Ti- and Fe-thresholds were found to be almost identical.

In Figure 5, it can be seen that for calcination temperatures up to 500 °C the mRDF of the 30% doped compound resembles that of the anatase reference, whereas for higher calcination temperatures, the spectra are basically identical to the one of pseudobrookite. Small deviations in the intensities result from changes of the (static) disorder of the neighboring ions. The peak heights in the mRDF are influenced by the root-mean square displacements of the atoms, which are described by the Debye−Waller factors. For crystalline samples the interatomic distances are well defined. Hence, the Debye−Waller factors are small and the mRDF peaks are rather high. Amorphous or nanoscopic materials, on the other hand, exhibit small and broad peaks in their mRDFs due to the large deviations of the interatomic distances. For nanoscopic materials these deviations derive from the strong influence of the surface, which locally disturbs the crystal lattice.

It is worth noting that the experimentally found mRDFs do not match those of Fe_2O_3 or Fe_3O_4. This is additional proof that iron is actually incorporated in the TiO_2 framework and no binary oxides are formed. The absence of a rutile-like radial distribution is consistent with the EPR results. It confirms that the amount of Fe incorporated into this TiO_2 phase must be very low and that almost the entire Fe reacts from a doped anatase to pseudobrookite within a small temperature regime of about 100 °C. The critical concentration of 0.2% Fe that, according to the EPR measurements, remains in the rutile phase is clearly too small to be detected by EXAFS spectroscopy.

As can be seen in Figure 5, the peak heights slightly increase with increasing calcination temperatures, reflecting a higher degree of structural order within the iron environment. At the same time, the line widths in the corresponding XRD patterns were found to decrease. Both effects can be explained by growing of the crystal grains upon heating.

Identical results were obtained for the samples with a 10% iron substitution. Again, for calcination temperatures up to 500 °C the Fe−K EXAFS was very similar to the anatase reference, while for higher temperatures a pseudobrookite-like absorption spectrum was observed. Apparently, in the high substitution regime the

(22) Teo, B. K. *EXAFS: Basic Principles and Data Analysis*; Springer: Berlin, 1986; Chapter 7.

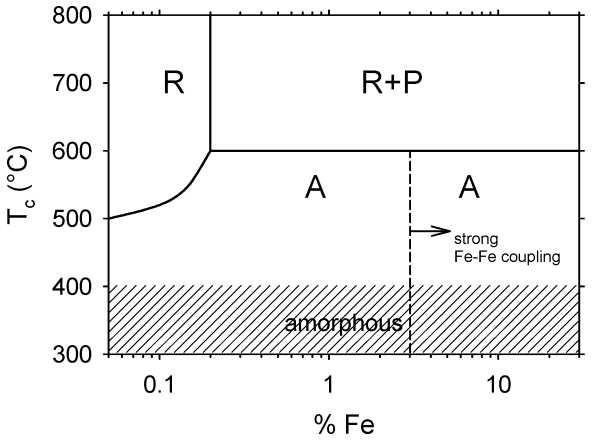

Figure 6. Kinetic phase diagram of nanostructured iron-doped titania from the butanediol sol−gel synthesis. Hatched areas correspond to poor crystalline quality. Phase transitions and segregations into mixed phases are indicated by red lines.

iron content does not significantly alter the thermal behavior of the samples.

Figure 6 gives a kinetic phase diagram of nanostructured iron-doped titania from the butanediol sol−gel synthesis derived by combining the results of the various complementary methods. For iron concentrations less than 0.2% the temperature of the phase transition from the anatase to the rutile structure increases with increasing iron concentration. Above this concentration the transition temperature remains approximately 600−650 °C. Samples calcinated at temperatures lower than 400 °C show poor crystalline quality and contain amorphous phases. At low calcination temperatures, the iron atoms are incorporated into the lattice of the anatase structure for Fe concentrations up to 30%. In contrast, only up to 0.2% Fe can be incorporated into rutile TiO_2.

Conclusions

We have presented a comprehensive kinetic phase diagram of TiO_2:Fe based on a butanediol sol−gel synthesis. The consistent picture has evolved as a result of the application of an appropriate set of complementary methods of investigation. We have clarified the Fe incorporation in TiO_2 from macroscopic to atomic scales. The flexibility of this synthesis pathway for Fe-doped titania allows one to control the material properties on atomic, mesoscopic, and macroscopic scales with respect to structure−morphology property relationships, i.e., to generate tailor-made functional materials.

CM034246P